






## Symmetry breaking and spectral structure of the interacting Hatano-Nelson model

Song-Bo Zhang <sup>1</sup>, M. Michael Denner <sup>1</sup>, Tomáš Bzdušek <sup>2,1</sup>, Michael A. Sentef <sup>3</sup> and Titus Neupert <sup>1</sup>

<sup>1</sup>*Department of Physics, University of Zürich, Winterthurerstrasse 190, 8057 Zürich, Switzerland*

<sup>2</sup>*Condensed Matter Theory Group, Paul Scherrer Institute, 5232 Villigen PSI, Switzerland*

<sup>3</sup>*Max Planck Institute for the Structure and Dynamics of Matter, Luruper Chaussee 149, 22761 Hamburg, Germany*



(Received 29 January 2022; revised 7 May 2022; accepted 22 August 2022; published 2 September 2022)

We study the Hatano-Nelson model, i.e., a one-dimensional non-Hermitian chain of spinless fermions with nearest-neighbor nonreciprocal hopping, in the presence of repulsive nearest-neighbor interactions. At half filling, we find two  $\mathcal{PT}$  transitions, as the interaction strength increases. The first transition is marked by an exceptional point between the first and the second excited state in a finite-size system and is a first-order symmetry-breaking transition into a charge-density wave regime. Persistent currents characteristic of the Hatano-Nelson model abruptly vanish at the transition. The second transition happens at a critical interaction strength that scales with the system size and can thus only be observed in finite-size systems. It is characterized by a collapse of all energy eigenvalues onto the real axis. We further show that in a strong interaction regime, but away from half filling, the many-body spectrum shows point gaps with nontrivial winding numbers, akin to the topological properties of the single-particle spectrum of the Hatano-Nelson chain, which indicates the skin effect of extensive many-body eigenstates under open boundary conditions. Our results can be applied to other models such as the non-Hermitian Su-Schrieffer-Heeger-type model and contribute to an understanding of fermionic many-body systems with non-Hermitian Hamiltonians.

DOI: [10.1103/PhysRevB.106.L121102](https://doi.org/10.1103/PhysRevB.106.L121102)

**Introduction.** Non-Hermitian topological phases constitute one of the most recent active research fields in condensed matter, cold atom, and photonic physics [1–33]. They have been experimentally realized in different platforms of high controllability [34–50]. So far, most previous efforts have been devoted to single-particle physics, with no or only perturbative many-body interactions. It is well known that in Hermitian systems strong interactions among particles give rise to many exotic phenomena, such as unconventional superconductivity, Mott insulators, and density-wave ordering [51–53]. Thus it is of fundamental interest to explore non-Hermitian phenomena in many-body systems with strong interactions [54–79]. Most of the existing studies on this subject are focused on the issues of non-Hermitian many-body localization [56–59] and the non-Hermitian skin effect [61–69]. However, many-body interaction effects, especially on bulk fermionic properties, remain largely unexplored even in simple models.

In this Letter, we study the Hatano-Nelson model of spinless fermions, a prototypical one-dimensional non-Hermitian system with nearest-neighbor nonreciprocal hopping [80], in a ring geometry and under the presence of the Pauli principle and strong Coulomb interactions. At half filling [Fig. 1(a)], we find that, as the interaction strength increases, the imaginary energies of the many-body spectrum are substantially suppressed, giving rise to two  $\mathcal{PT}$  transitions. The first transition is marked by an exceptional point between two lowest excited states (LES) [81] of a finite-size system [see a sketch in Fig. 1(b)]. By employing exact diagonalization, we show that this transition corresponds to a first-order quantum phase transition of the ground state from a gapless phase to a gapped

charge-density wave (CDW) that breaks translation symmetry spontaneously [Fig. 1(c)]. Moreover, it features a sudden disappearance of the characteristic persistent current of the Hatano-Nelson model in a low-temperature regime. The second transition corresponds to a full collapse of the many-body spectrum onto the real axis. Its critical interaction strength, however, increases as the system size grows. Thus it can only be observed in finite-size systems.

For finite doping away from half filling, the spectrum stratifies into clusters with states of a different number of simultaneously occupied nearest-neighbor sites. The energy clusters have nonzero extents along the imaginary axis being largely unaffected by interactions. Furthermore, they exhibit point gaps with nontrivial winding numbers, thus indicating the skin effect of many-body states in the presence of open boundaries [13–15,82], also for strong interactions. At half filling, in contrast, the spectrum shrinks to open lines under strong interactions. Accordingly, the many-body states extend over the whole lattice chain with open boundaries.

**Interacting Hatano-Nelson model.** We consider the interacting Hatano-Nelson model of spinless fermions described by

$$\hat{H} = \sum_{\ell} [(t + \gamma)\hat{c}_{\ell}^{\dagger}\hat{c}_{\ell+1} + (t - \gamma)\hat{c}_{\ell+1}^{\dagger}\hat{c}_{\ell} + U\hat{n}_{\ell}\hat{n}_{\ell+1}], \quad (1)$$

where  $\hat{c}_{\ell}^{\dagger}$  ( $\hat{c}_{\ell}$ ) is the creation (annihilation) operator of a fermion at lattice site  $\ell$  and  $\hat{n}_{\ell} = \hat{c}_{\ell}^{\dagger}\hat{c}_{\ell}$  is the fermion number operator with eigenvalues  $\{0, 1\}$ . The fermionic operators  $\hat{c}_{\ell}^{\dagger}$  and  $\hat{c}_{\ell}$  obey the anticommutation relations, thus imposing

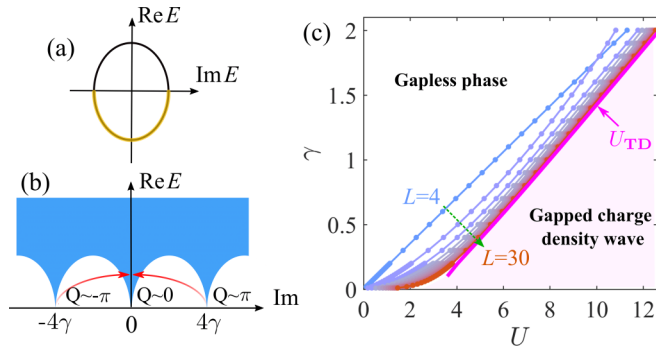


FIG. 1. (a) Single-particle spectrum and (b) low-excitation-energy many-body spectrum at half filling in the absence of interactions. The yellow arc denotes the filled states. Two LES have momenta  $Q = \pm\pi$  and identical  $\text{Re}(E)$  but opposite  $\text{Im}(E) \approx \pm 4i\gamma$ . By increasing the interaction strength  $U$  to a critical value  $U_c$ , the two LES collapse onto the real axis, as sketched by the arrows. (c) Phase diagram against  $\gamma$  and  $U$ . The gapless phase is adiabatically connected to the Hatano-Nelson model at  $U = 0$ , while the CDW phase is smoothly connected to the CDW phase with  $\gamma = 0$  and finite  $U$ . The magenta line is the extrapolated  $U_{\text{TD}}$  in the TDL. It demarcates the gapless regime and the gapped CDW regime.

the Pauli principle to the system [84]. The real parameters  $t$  and  $\gamma$  denote the reciprocal and nonreciprocal components of the hopping between neighboring sites, respectively [85]. The last term describes the Coulomb interaction with strength  $U \geq 0$  between two fermions at adjacent sites. Without loss of generality, we set  $t > 0$  to be our unit of energy.

To investigate bulk many-body properties, we consider the system in a ring geometry with  $L$  sites and  $N$  particles. For periodic boundary conditions (PBC) or anti-PBC, the system respects a combined space-time-reversal ( $\mathcal{PT}$ ) symmetry [84]; thus the eigenenergies of the system are either real or come in complex-conjugate pairs. For single particles without interactions, the spectrum reduces to a closed orbit with a point gap [Fig. 1(a)], resulting in the non-Hermitian skin effect of single-particle states at open boundaries [4–6]. Moreover, the system has a particle-hole symmetry [84]. Thus the spectrum for  $N$  particles is essentially the same (up to an overall shift in energy) as that for  $L - N$  particles. Both of these spectral relations are reproduced by our exact-diagonalization calculations presented below.

**Low-energy  $\mathcal{PT}$  transition and phase diagram.** It is instructive to first analyze the case without interactions ( $U = 0$ ). In this case, the many-body spectrum displays a scatter distribution pattern centered at the origin of the complex-energy plane. When  $n_{\text{cl}} = \min(N, L - N) \gg 1$ , its extent along real and imaginary axes can be estimated as  $\Xi_{\text{R}} \approx t\alpha_{\{N,L\}}$  and  $\Xi_{\text{I}} \approx \gamma\alpha_{\{N,L\}}$ , respectively, where  $\alpha_{\{N,L\}} = 2L \sin(\pi n_{\text{cl}}/L)/\pi$  [84]. Clearly, the spectrum is larger when the system is larger and filled closer to half filling. For fixed finite  $n_{\text{cl}} (\ll L)$ , however, its extent is approximately independent of  $L$  and determined by  $\alpha_{\{N,L\}} \approx 2n_{\text{cl}}$ .

More intriguing features arise when the interaction is present. We first consider the half filled ( $N = L/2$ ) scenario and show that a  $\mathcal{PT}$  transition between  $\mathcal{PT}$ -symmetry-broken and -unbroken phases occurs at low excitation energies, as

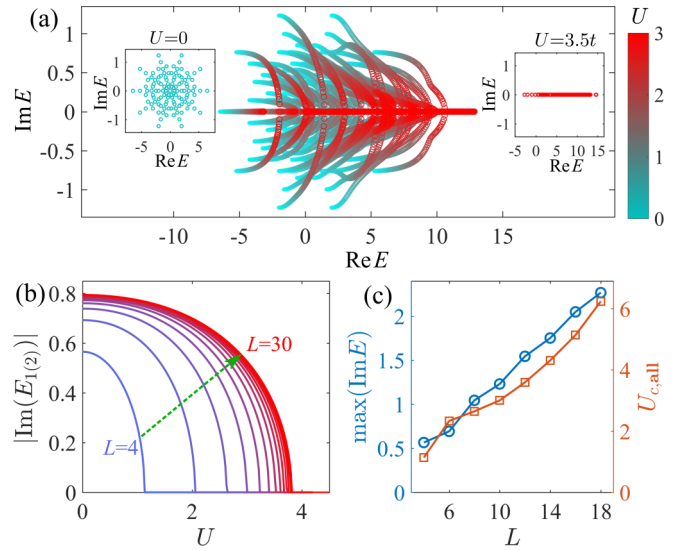


FIG. 2. (a) Flow of the spectrum at half filling as  $U$  increases from 0 (cyan) to  $3.5t$  (red). Inset: spectra at  $U = 0$  and  $U = 3t$ , respectively. All eigenenergies become real when  $U \geq U_{c,\text{all}}$ . (b)  $|\text{Im}(E_{1(2)})|$  as a function of  $U$  for increasing  $L$ . The dependence of  $|\text{Im}(E_{1(2)})|$  on  $U$  converges to the red curve as  $L$  grows. (c) Maximum imaginary energy  $\max(\text{Im} E)$  (blue) and  $U_{c,\text{all}}$  (orange) as functions of  $L$ . Both quantities diverge as  $L \rightarrow \infty$ . We consider  $L = 10$  in (a),  $\gamma = 0.2t$  in all panels, and adopt (anti-)PBC for odd (even)  $N$ .

$U$  increases. As illustrated in Fig. 1(b) and the inset of Fig. 2(a), at  $U = 0$ , there is one ground state with real energy  $E_0$  and two LES with complex-conjugate energies  $E_2 = E_1^*$  in systems with odd (even)  $N$  and (anti-)PBC. When  $L \gg 1$ , we have  $E_0 \approx 2tL/\pi$  and  $E_1 = E_2^* \approx E_0 + 4t \sin(\pi/L) + 4i\gamma \cos(\pi/L)$ . As  $U$  increases, we find that the energies of the LES approach each other and merge at an exceptional point on the real axis at a critical strength  $U = U_c$  and split along the real axis for  $U > U_c$ .

To better understand the *low-energy*  $\mathcal{PT}$  transition, we determine  $U_c$  for varying  $\gamma$  and increasing  $L$  [Figs. 1(c) and 2(b)]. Evidently,  $|\text{Im}(E_{1(2)})|$  decays monotonically with increasing  $U (< U_c)$  and completely vanishes when  $U > U_c$ . As  $L$  grows, the dependence of  $|\text{Im}(E_{1(2)})|$  on  $U$  converges to a curve [red line in Fig. 2(b)]. In the thermodynamic limit (TDL)  $L \rightarrow \infty$ ,  $U_c$  converges to a finite value  $U_{\text{TD}}$ . Specifically, for fixed  $\gamma$ ,  $U_c$  shows a power-law scaling as  $L$  grows, i.e.,

$$U_c = U_{\text{TD}} - \beta L^{-\alpha}, \quad (2)$$

where  $\alpha$  and  $\beta$  are positive numbers depending on  $\gamma$ . This feature enables us to extrapolate  $U_{\text{TD}}$ . The phase diagram parametrized by  $U$  and  $\gamma$  is given in Fig. 1(c), where the red line is  $U_{\text{TD}}$  which marks the phase boundary in the TDL [86]. We observe that  $U_{\text{TD}}$  grows monotonically with  $\gamma$ , indicating that the  $\mathcal{PT}$  transition occurs even in the TDL and for ultrastrong nonreciprocity ( $|\gamma| \geq t$ ). More details of the calculation are given in the Supplemental Material [84].

To further understand the physics behind the phase diagram, we analyze the real part of the low-excitation-energy spectrum [Fig. 3(a)]. For  $U < U_c$ , the two LES are degenerate in real energy. The finite-size level spacing  $\Delta_{01} \equiv \text{Re}(E_1 -$

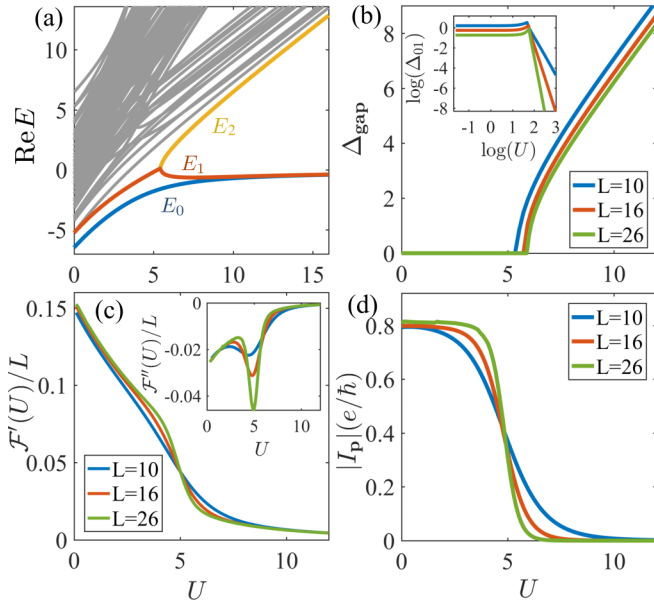


FIG. 3. (a) Real part of the spectrum at half filling as a function of  $U$ . Three lowest energy levels are respectively denoted as  $E_0$ ,  $E_1$ , and  $E_2$ . (b)  $\Delta_{\text{gap}}$  as a function of  $U$ . Inset:  $\ln(\Delta_{01})$  as a function of  $\ln(U)$ . (c) The first and second (inset) derivatives of the free energy as functions of  $U$ . (d)  $|I_p|$  (in units of  $e/\hbar$ ) as a function of  $U$ . We consider  $\gamma = 0.6t$  in all panels,  $L = 10$  in (a), and  $k_B T = 0.4t$  and 50 lowest- $\text{Re}(E)$  eigenstates in (c) and (d).

$E_0$  is approximately constant [ $\approx 4t \sin(2\pi/L)$ ] for a wide range of  $U$  and increases subtly when approaching  $U_c$  [inset of Fig. 3(b)]. However,  $\Delta_{01}$  decreases as  $L$  grows and it vanishes in the TDL, indicating a gapless phase when  $U < U_c$ . For  $U > U_c$ , the LES have vanishing imaginary energy while being split in real energy. Upon further increasing  $U$ , the energy splitting  $\Delta_{\text{gap}} \equiv \text{Re}(E_2 - E_1)$  increases, whereas  $\Delta_{01}$  decreases sharply [Fig. 3(b)]. More explicitly,  $\Delta_{01}$  follows a power-law dependence  $\Delta_{01} \propto U^{1-L/2}$  on  $L$ . Thus, in large systems, one of the LES rapidly becomes degenerate with the ground state and separated from the excited states by a large gap  $\Delta_{\text{gap}}$ , implying a transition of the system into a gapped regime. The degenerate ground states break translation symmetry spontaneously, forming a CDW with long-range density-density correlation [84]. The  $\mathcal{PT}$  transition may also be related to the breakdown of the Mott insulator which instead considers two spin species and on-site interactions [83].

*Free energy and persistent current.* Next, we consider the free energy of the system, which reads  $\mathcal{F} = -k_B T \ln(\sum_j e^{-E_j/k_B T})$ , where  $T$  is the temperature,  $k_B$  is the Boltzmann constant, and  $\sum_j$  sums over all eigenenergies. Since the eigenenergies are real or come in complex-conjugate pairs due to the  $\mathcal{PT}$  symmetry,  $\mathcal{F}$  is always purely real. At low temperatures,  $\mathcal{F}$  is determined mainly by the low- $\text{Re}(E)$  eigenstates in an energy window of magnitude  $k_B T$ . As discussed above, in the TDL, the system is gapless for  $U < U_c$ , whereas it quickly develops a large energy gap after  $U > U_c$ . As a result,  $\mathcal{F}$  and its derivatives (with respect to  $U$ ) change significantly at  $U_c$ , provided that  $\Delta_{01} < k_B T \ll U_c$ . In Fig. 3(c), we calculate the first and second derivatives of  $\mathcal{F}$  at low temperatures as functions of  $U$ . We observe that,

$L/2 \gg 1$ , the first derivative  $\mathcal{F}' \equiv d\mathcal{F}/dU$  shows a sudden drop while the second derivative  $\mathcal{F}'' \equiv d^2\mathcal{F}/dU^2$  diverges at  $U_c$ . These features are more pronounced in larger systems, suggesting that the low-energy  $\mathcal{PT}$  transition is of first order. This is in sharp contrast to the Hermitian limit ( $\gamma = 0$ ), where the transition is of Berezinskii-Kosterlitz-Thouless type [87–89] (see also [84]).

In a metallic ring, a persistent current  $I_p$  can be induced as the response of  $\mathcal{F}$  to a small change of magnetic flux  $\phi$  through the ring, i.e.,  $I_p = -(e/\hbar)\partial\mathcal{F}/\partial\phi$  [90]. Notably, by virtue of its non-Hermitian hopping, the Hatano-Nelson model supports an imaginary current  $I_p$  at zero flux for  $U < U_c$  [91]. In the TDL and for  $U = 0$  and  $T = 0$ ,  $I_p$  can be derived as  $I_p = 4ie\gamma/h$  [84]. Moreover, when  $\Delta_{01} < k_B T \ll U_c$ ,  $I_p$  is approximately constant for  $U < U_c$ , whereas it suddenly drops to zero for  $U > U_c$ , as shown numerically in Fig. 3(d). For small  $U$ ,  $I_p$  saturates for large  $L$ , and it exhibits a sudden drop at the transition that sharpens with increasing  $L$ . This is in contrast to the persistent current in Hermitian systems that requires a finite flux and vanishes in the TDL [92]. Note that the imaginary current characterizes the delocalization of eigenstates [80]. The sudden disappearance of  $I_p$  thus constitutes another indicator of the metal-insulator transition in the low- $\text{Re}(E)$  regime.

*$\mathcal{PT}$  transition in the full spectrum.* The full many-body spectrum can also exhibit a  $\mathcal{PT}$  transition at half filling. As shown in Fig. 2(a) for  $|\gamma| < t$ , the imaginary part of the spectrum is dramatically suppressed by increasing  $U$  and, more remarkably, all eigenenergies collapse onto the real axis after a critical strength  $U_{c,\text{all}}$  in a system with odd (even)  $N$  and (anti-)PBC. This *full*  $\mathcal{PT}$  transition can be understood as follows. In the presence of Coulomb interactions, the many-body Fock states of the system acquire different Coulomb potentials determined by their occupation configurations [93], forming different groups with different Coulomb potentials (we term them Fock components for convenience). At half filling, we find that the imaginary energies of the spectrum mainly stem from the nonreciprocal hopping between different Fock components. By increasing  $U$ , the energy separation between the Fock components grows and the coupling between them becomes weaker. Thus the imaginary energies are suppressed. We stress that the complex-real transition discovered here emerges in the many-body spectrum and is driven by two-particle interactions, distinctively different from the complex-real transition in the single-particle spectrum driven by disorders [80].

The value of  $U_{c,\text{all}}$  depends on the system size  $L$  and non-reciprocity  $\gamma$ . In larger systems, there are more excited states with larger imaginary energies at  $U = 0$ . When  $L \gg 1$ , the maximum imaginary energy  $\max[\text{Im}(E)]$  is approximately  $2\gamma L/\pi$ , which grows linearly with  $L$  [in contrast to the imaginary energies of LES, which is bounded by  $\text{Im}(E_1) < 4\gamma$ ]. Thus, in order to completely suppress the imaginary energies, a stronger  $U_{c,\text{all}}$  is required. Explicitly,  $U_{c,\text{all}}$  scales with the system size and can thus only be observed in finite-size systems [Fig. 2(c)]. Similarly, for larger  $\gamma$ , we have larger imaginary energies at  $U = 0$  and thus larger  $U_{c,\text{all}}$ .

For  $|\gamma| \geq t$ , the imaginary energies stem not only from the nonreciprocal hopping between different Fock components but also from those between the states within the same

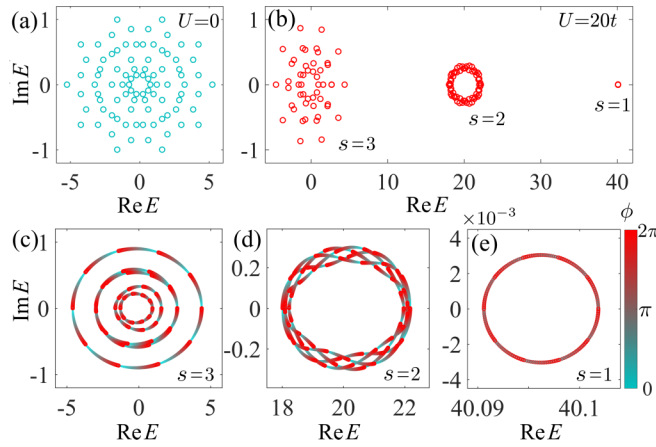


FIG. 4. Many-body spectrum at (a)  $U = 0$  and (b)  $20t$ , respectively. (c)–(e) Movement of the spectral clusters as  $\phi$  varies from 0 (cyan) to  $2\pi$  (red). Parameters:  $L = 10$ ,  $N = 3$ , and  $\gamma = 0.2t$

component. Since these hoppings are not suppressed by the  $U$ -driven separation of the Fock components, the imaginary energies are a robust property and the full  $\mathcal{PT}$  transition is not realized at any finite  $U$ .

We also note that the above-discussed  $\mathcal{PT}$  transitions occur only in the case with odd (even)  $N$  and (anti-)PBC while they are absent in the case with even (odd)  $N$  and (anti-)PBC. However, we expect the phase diagram in the TDL to be identical for all the cases [84].

*Spectral clusters with nontrivial windings away from half filling.* Finally, we turn to the non-half-filled case where additional interesting properties emerge in the presence of strong interactions. First, the many-body spectrum is substantially redistributed and dispersed from a connected area in the complex-energy plane into  $n_{cl}$  clusters when  $U > \Xi_R$  [Figs. 4(a) and 4(b)]. Each cluster corresponds to a Fock component with a given Coulomb potential. Accordingly, the clusters are centered respectively around the energies  $\varepsilon_s = (N - s)U$  with  $1 \leq s \leq n_{cl}$  labeling the clusters. Second, each cluster by itself also exhibits a symmetric pattern in the complex-energy plane. Due to particle-hole symmetry, the clusters for  $L - N$  particles are the same as those for  $N$  particles up to an overall energy shift  $|2N - L|U$ . Finally, in the non-half-filled case, the imaginary energies always comprise nonreciprocal hopping between states within the same Fock component. Thus the clusters are insensitive to  $U$  in the strong  $U$  regime, except for the cluster centered at  $\varepsilon_1$ , whose extent shrinks with increasing  $U$ .

The spectral clusters can be characterized by nontrivial topological invariants. To see this, for finite-size systems, we introduce a twist angle  $\phi$  to the PBC [8]. When  $\phi$  increases from 0 to  $2\pi$ , all the eigenenergies belonging to cluster  $s$  wind around the center  $\varepsilon_s$  in one direction determined by  $\text{sgn}(\gamma)$  [Figs. 4(c)–4(e)]. Thus a nontrivial winding number can be found as

$$v_s = \int_0^{2\pi} \frac{d\phi}{2\pi i} \sum_j \partial_\phi \ln \{E_j(\phi) - \varepsilon_s\}, \quad (3)$$

where  $\sum_j$  sums over all eigenenergies. Specifically, we find  $v_1 = \text{sgn}(\gamma)N$  for  $s = 1$ . For other clusters  $s \geq 2$ ,  $v_s$  depend also on  $L$  and diverge as  $L \rightarrow \infty$ . Furthermore, for fixed  $N$  in the TDL, the clusters form at least one continuous orbit of eigenenergies surrounding each energy center [84]. Hence the winding numbers of these orbits can also define nontrivial topological invariants. Note that the winding numbers defined for the spectral clusters are general for strong interactions  $U > \Xi_R$  [94]. The spectrum under open boundary conditions collapses to open lines without windings. The nonzero winding numbers under PBC indicate the localization of the many-body eigenstates at the Fock basis states with particles accumulated at an open boundary (if present) and hence the localization of the many-body eigen wave functions towards the boundary [62,69,95], regardless of the Pauli principle and strong interactions in the system. We show this explicitly in the Supplemental Material [84]. Our work thus constitutes a many-body interacting generalization of the spectral winding number [13–15,82] used to characterize the non-Hermitian skin effect.

By contrast, at half filling, the spectrum of a finite-size system under PBC shrinks to open lines in the strong interaction regime, as discussed before. In this case, the spectral winding numbers become ill defined. The many-body wave functions extend over the whole lattice even with boundaries [84].

*Summary and discussion.* We have revealed two  $\mathcal{PT}$  transitions in the interacting Hatano-Nelson model at half filling upon increasing interaction strength: one is marked by an exceptional point between two LES and the other one is characterized by a full collapse of the many-body spectrum onto the real axis. The former transition corresponds to a symmetry-breaking transition into a gapped CDW regime and features a sudden disappearance of the persistent current at low temperatures. We have further shown that, with strong interactions but away from half filling, the many-body spectrum stratifies into multiple clusters characterized by nontrivial winding numbers.

It is important to note that our main results from the Hatano-Nelson model are general. They can also be applied to other models, such as the Su-Schrieffer-Heeger (SSH) type model that has nonreciprocal hopping for every two nearest-neighbor bonds, as we have verified in the Supplemental Material [84]. Our theory may be implemented, for instance, in open quantum dot [102–105], cold-atom [28,48–50,106–108], and monitored quantum circuit systems [109,110].

*Note added in proof.* Recently, we noticed the related work [111], which focuses on the spectral winding and non-Hermitian skin effect.

*Acknowledgments.* We thank F. Alsallom, N. Astrakhantsev, M. Brzezińska, J. Budich, X.-D. Cao, S.-J. Choi, C. Li, L. Herviou, W. Rui, G. Tang, A. Tiwari, and O. V. Yazyev for valuable discussions. This work was supported by the European Research Council (ERC) under the European Union’s Horizon 2020 research and innovation program (ERC-StG-Neupert-757867-PARATOP) and from NCCR MARVEL funded by the SNSF. M.S. was supported by DFG through the Emmy Noether program (SE 2558/2). T.B. was supported by the Ambizione Grant No. 185806 by the Swiss National Science Foundation.

- [1] H. Shen, B. Zhen, and L. Fu, Topological Band Theory for Non-Hermitian Hamiltonians, *Phys. Rev. Lett.* **120**, 146402 (2018).
- [2] V. Kozii and L. Fu, Non-Hermitian Topological Theory of Finite-Lifetime Quasiparticles: Prediction of Bulk Fermi Arc Due to Exceptional Point, [arXiv:1708.05841](https://arxiv.org/abs/1708.05841).
- [3] A. A. Zyuzin and A. Y. Zyuzin, Flat band in disorder-driven non-Hermitian Weyl semimetals, *Phys. Rev. B* **97**, 041203(R) (2018).
- [4] S. Yao and Z. Wang, Edge States and Topological Invariants of Non-Hermitian Systems, *Phys. Rev. Lett.* **121**, 086803 (2018).
- [5] F. K. Kunst, E. Edvardsson, J. C. Budich, and E. J. Bergholtz, Biorthogonal Bulk-Boundary Correspondence in Non-Hermitian Systems, *Phys. Rev. Lett.* **121**, 026808 (2018).
- [6] T. E. Lee, Anomalous Edge State in a Non-Hermitian Lattice, *Phys. Rev. Lett.* **116**, 133903 (2016).
- [7] S. Yao, F. Song, and Z. Wang, Non-Hermitian Chern Bands, *Phys. Rev. Lett.* **121**, 136802 (2018).
- [8] Z. Gong, Y. Ashida, K. Kawabata, K. Takasan, S. Higashikawa, and M. Ueda, Topological Phases of Non-Hermitian Systems, *Phys. Rev. X* **8**, 031079 (2018).
- [9] L. E. F. Foa Torres, Perspective on topological states of non-Hermitian lattices, *J. Phys. Mater.* **3**, 014002 (2020).
- [10] Y. Ashida, Z. Gong, and M. Ueda, Non-hermitian physics, *Adv. Phys.* **69**, 249 (2020).
- [11] M.-A. Miri and A. Alu, Exceptional points in optics and photonics, *Science* **363**, eaar7709 (2019).
- [12] E. J. Bergholtz, J. C. Budich, and F. K. Kunst, Exceptional topology of non-Hermitian systems, *Rev. Mod. Phys.* **93**, 015005 (2021).
- [13] K. Kawabata, K. Shiozaki, M. Ueda, and M. Sato, Symmetry and Topology in Non-Hermitian Physics, *Phys. Rev. X* **9**, 041015 (2019).
- [14] K. Zhang, Z. Yang, and C. Fang, Correspondence between Winding Numbers and Skin Modes in Non-Hermitian Systems, *Phys. Rev. Lett.* **125**, 126402 (2020).
- [15] N. Okuma, K. Kawabata, K. Shiozaki, and M. Sato, Topological Origin of Non-Hermitian Skin Effects, *Phys. Rev. Lett.* **124**, 086801 (2020).
- [16] D. Leykam, K. Y. Bliokh, C. Huang, Y. D. Chong, and F. Nori, Edge Modes, Degeneracies, and Topological Numbers in Non-Hermitian Systems, *Phys. Rev. Lett.* **118**, 040401 (2017).
- [17] V. M. Martinez Alvarez, J. E. Barrios Vargas, and L. E. F. Foa Torres, Non-Hermitian robust edge states in one dimension: Anomalous localization and eigenspace condensation at exceptional points, *Phys. Rev. B* **97**, 121401(R) (2018).
- [18] S. Lieu, Topological phases in the non-Hermitian Su-Schrieffer-Heeger model, *Phys. Rev. B* **97**, 045106 (2018).
- [19] Y. Xiong, Why does bulk boundary correspondence fail in some non-Hermitian topological models, *J. Phys. Commun.* **2**, 035043 (2018).
- [20] T. Yoshida, R. Peters, and N. Kawakami, Non-Hermitian perspective of the band structure in heavy-fermion systems, *Phys. Rev. B* **98**, 035141 (2018).
- [21] W. B. Rui, M. M. Hirschmann, and A. P. Schnyder,  $\mathcal{PT}$ -symmetric non-Hermitian Dirac semimetals, *Phys. Rev. B* **100**, 245116 (2019).
- [22] S. Longhi, Topological Phase Transition in Non-Hermitian Quasicrystals, *Phys. Rev. Lett.* **122**, 237601 (2019).
- [23] C. H. Lee and R. Thomale, Anatomy of skin modes and topology in non-Hermitian systems, *Phys. Rev. B* **99**, 201103(R) (2019).
- [24] K. Kawabata, T. Bessho, and M. Sato, Classification of Exceptional Points and Non-Hermitian Topological Semimetals, *Phys. Rev. Lett.* **123**, 066405 (2019).
- [25] T. Yoshida, R. Peters, N. Kawakami, and Y. Hatsugai, Symmetry-protected exceptional rings in two-dimensional correlated systems with chiral symmetry, *Phys. Rev. B* **99**, 121101(R) (2019).
- [26] J. Y. Lee, J. Ahn, H. Zhou, and A. Vishwanath, Topological Correspondence between Hermitian and Non-Hermitian Systems: Anomalous Dynamics, *Phys. Rev. Lett.* **123**, 206404 (2019).
- [27] D. S. Borgnia, A. J. Kruchkov, and R.-J. Slager, Non-Hermitian Boundary Modes and Topology, *Phys. Rev. Lett.* **124**, 056802 (2020).
- [28] L. Li, C. H. Lee, and J. Gong, Topological Switch for Non-Hermitian Skin Effect in Cold-Atom Systems with Loss, *Phys. Rev. Lett.* **124**, 250402 (2020).
- [29] C. C. Wojcik, X.-Q. Sun, T. Bzdušek, and S. Fan, Homotopy characterization of non-Hermitian Hamiltonians, *Phys. Rev. B* **101**, 205417 (2020).
- [30] M. M. Denner, A. Skurativska, F. Schindler, M. H. Fischer, R. Thomale, T. Bzdušek, and T. Neupert, Exceptional topological insulators, *Nat. Commun.* **12**, 5681 (2021).
- [31] P. M. Vecsei, M. M. Denner, T. Neupert, and F. Schindler, Symmetry indicators for inversion-symmetric non-Hermitian topological band structures, *Phys. Rev. B* **103**, L201114 (2021).
- [32] F. Schindler and A. Prem, Dislocation non-Hermitian skin effect, *Phys. Rev. B* **104**, L161106 (2021).
- [33] J.-W. Ryu, N. Myoung, A. Go, S. Woo, S.-J. Choi, and H. C. Park, Emergent localized states at the interface of a twofold  $\mathcal{PT}$ -symmetric lattice, *Phys. Rev. Research* **2**, 033149 (2020).
- [34] W. Chen, Ş. K. Özdemir, G. Zhao, J. Wiersig, and L. Yang, Exceptional points enhance sensing in an optical microcavity, *Nature (London)* **548**, 192 (2017).
- [35] H. Hodaei, A. U. Hassan, S. Wittek, H. Garcia-Gracia, R. El-Ganainy, D. N. Christodoulides, and M. Khajavikhan, Enhanced sensitivity at higher-order exceptional points, *Nature (London)* **548**, 187 (2017).
- [36] S. Weimann, M. Kremer, Y. Plotnik, Y. Lumer, S. Nolte, K. G. Makris, M. Segev, M. C. Rechtsman, and A. Szameit, Topologically protected bound states in photonic parity-time-symmetric crystals, *Nat. Mater.* **16**, 433 (2017).
- [37] H. Zhou, C. Peng, Y. Yoon, C. W. Hsu, K. A. Nelson, L. Fu, J. D. Joannopoulos, M. Soljačić, and B. Zhen, Observation of bulk Fermi arc and polarization half charge from paired exceptional points, *Science* **359**, 1009 (2018).
- [38] H. Zhao, X. Qiao, T. Wu, B. Midya, S. Longhi, and L. Feng, Non-Hermitian topological light steering, *Science* **365**, 1163 (2019).
- [39] A. Cerjan, S. Huang, M. Wang, K. P. Chen, Y. Chong, and M. C. Rechtsman, Experimental realization of a Weyl exceptional ring, *Nat. Photon.* **13**, 623 (2019).
- [40] T. Helbig, T. Hofmann, S. Imhof, M. Abdelghany, T. Kiessling, L. Molenkamp, C. Lee, A. Szameit, M. Greiter, and R. Thomale, Generalized bulk-boundary correspondence

- in non-Hermitian topoelectrical circuits, *Nat. Phys.* **16**, 747 (2020).
- [41] S. Weidemann, M. Kremer, T. Helbig, T. Hofmann, A. Stegmaier, M. Greiter, R. Thomale, and A. Szameit, Topological funneling of light, *Science* **368**, 311 (2020).
- [42] L. Xiao, T. Deng, K. Wang, G. Zhu, Z. Wang, W. Yi, and P. Xue, Non-Hermitian bulk–boundary correspondence in quantum dynamics, *Nat. Phys.* **16**, 761 (2020).
- [43] A. Ghatak, M. Brandenbourger, J. van Wezel, and C. Coulais, Observation of non-Hermitian topology and its bulk–edge correspondence in an active mechanical metamaterial, *Proc. Natl. Acad. Sci. USA* **117**, 29561 (2020).
- [44] W. Zhang, X. Ouyang, X. Huang, X. Wang, H. Zhang, Y. Yu, X. Chang, Y. Liu, D.-L. Deng, and L.-M. Duan, Observation of Non-Hermitian Topology with Nonunitary Dynamics of Solid-State Spins, *Phys. Rev. Lett.* **127**, 090501 (2021).
- [45] S. Xia, D. Kaltsas, D. Song, I. Komis, J. Xu, A. Szameit, H. Buljan, K. G. Makris, and Z. Chen, Nonlinear tuning of PT symmetry and non-Hermitian topological states, *Science* **372**, 72 (2021).
- [46] R. Su, E. Estrecho, D. Biegańska, Y. Huang, M. Wurdack, M. Pieczarka, A. G. Truscott, T. C. H. Liew, E. A. Ostrovskaya, and Q. Xiong, Direct measurement of a non-Hermitian topological invariant in a hybrid light-matter system, *Sci. Adv.* **7**, eabj8905 (2021).
- [47] K. Wang, A. Dutt, K. Y. Yang, C. C. Wojcik, J. Vucković, and S. Fan, Generating arbitrary topological windings of a non-Hermitian band, *Science* **371**, 1240 (2021).
- [48] W. Gou, T. Chen, D. Xie, T. Xiao, T. S. Deng, B. Gadway, W. Yi, and B. Yan, Tunable Nonreciprocal Quantum Transport through a Dissipative Aharonov-Bohm Ring in Ultracold Atoms, *Phys. Rev. Lett.* **124**, 070402 (2020).
- [49] Q. Liang, D. Xie, Z. Dong, H. Li, Z. Gadway, W. Yi, and B. Yan, Observation of Non-Hermitian Skin Effect and Topology in Ultracold Atoms, *Phys. Rev. Lett.* **129**, 070401 (2022).
- [50] Z. Ren, D. Liu, E. Zhao, C. He, K. K. Pak, J. Li, and G. B. Jo, Chiral control of quantum states in non-Hermitian spin–orbit-coupled fermions, *Nat. Phys.* **18**, 385 (2022).
- [51] F. Haldane, ‘Luttinger liquid theory’ of one-dimensional quantum fluids. I. Properties of the Luttinger model and their extension to the general 1D interacting spinless Fermi gas, *J. Phys. C: Solid State Phys.* **14**, 2585 (1981).
- [52] T. Giamarchi, *Quantum Physics in One Dimension* (Clarendon Press, Oxford, 2003), Vol. 121.
- [53] E. Fradkin, *Field Theories of Condensed Matter Physics* (Cambridge University Press, Cambridge, UK, 2013).
- [54] M. Nakagawa, N. Kawakami, and M. Ueda, Non-Hermitian Kondo Effect in Ultracold Alkaline-Earth Atoms, *Phys. Rev. Lett.* **121**, 203001 (2018).
- [55] T. Yoshida, K. Kudo, and Y. Hatsugai, Non-Hermitian fractional quantum Hall states, *Sci. Rep.* **9**, 16895 (2019).
- [56] R. Hamazaki, K. Kawabata, and M. Ueda, Non-Hermitian Many-Body Localization, *Phys. Rev. Lett.* **123**, 090603 (2019).
- [57] G.-Q. Zhang, D.-W. Zhang, Z. Li, Z. D. Wang, and S.-L. Zhu, Statistically related many-body localization in the one-dimensional anyon Hubbard model, *Phys. Rev. B* **102**, 054204 (2020).
- [58] L.-J. Zhai, S. Yin, and G.-Y. Huang, Many-body localization in a non-Hermitian quasiperiodic system, *Phys. Rev. B* **102**, 064206 (2020).
- [59] N. Fayard, L. Henriot, A. Asenjo-Garcia, and D. E. Chang, Many-body localization in waveguide quantum electrodynamics, *Phys. Rev. Research* **3**, 033233 (2021).
- [60] K. Yamamoto, M. Nakagawa, K. Adachi, K. Takasan, M. Ueda, and N. Kawakami, Theory of Non-Hermitian Fermionic Superfluidity with a Complex-Valued Interaction, *Phys. Rev. Lett.* **123**, 123601 (2019).
- [61] E. Lee, H. Lee, and B.-J. Yang, Many-body approach to non-Hermitian physics in fermionic systems, *Phys. Rev. B* **101**, 121109(R) (2020).
- [62] S. Mu, C. H. Lee, L. Li, and J. Gong, Emergent Fermi surface in a many-body non-Hermitian fermionic chain, *Phys. Rev. B* **102**, 081115(R) (2020).
- [63] D.-W. Zhang, Y.-L. Chen, G.-Q. Zhang, L.-J. Lang, Z. Li, and S.-L. Zhu, Skin superfluid, topological Mott insulators, and asymmetric dynamics in an interacting non-Hermitian Aubry-André-Harper model, *Phys. Rev. B* **101**, 235150 (2020).
- [64] T. Liu, J. J. He, T. Yoshida, Z.-L. Xiang, and F. Nori, Non-Hermitian topological Mott insulators in one-dimensional fermionic superlattices, *Phys. Rev. B* **102**, 235151 (2020).
- [65] A. Panda and S. Banerjee, Entanglement in nonequilibrium steady states and many-body localization breakdown in a current-driven system, *Phys. Rev. B* **101**, 184201 (2020).
- [66] N. Okuma and M. Sato, Non-Hermitian Skin Effects in Hermitian Correlated or Disordered Systems: Quantities Sensitive or Insensitive to Boundary Effects and Pseudo-Quantum-Number, *Phys. Rev. Lett.* **126**, 176601 (2021).
- [67] T. Yoshida, Real-space dynamical mean field theory study of non-Hermitian skin effect for correlated systems: Analysis based on pseudospectrum, *Phys. Rev. B* **103**, 125145 (2021).
- [68] K. Cao, Q. Du, X.-R. Wang, and S.-P. Kou, Physics of Many-body Nonreciprocal Model: Quantum System with Maxwell’s Pressure Demon, [arXiv:2109.03690](https://arxiv.org/abs/2109.03690).
- [69] F. Alsallom, L. Herviou, O. V. Yazyev, and M. Brzezińska, Fate of the non-Hermitian skin effect in many-body fermionic systems, *Phys. Rev. Research* **4**, 033122 (2022).
- [70] A. Y. Guo, S. Lieu, M. C. Tran, and A. V. Gorshkov, Clustering of steady-state correlations in open systems with long-range interactions, [arXiv:2110.15368](https://arxiv.org/abs/2110.15368).
- [71] Y.-G. Liu, L. Xu, and Z. Li, Quantum phase transition in a non-Hermitian XY spin chain with global complex transverse field, *J. Phys.: Condens. Matter* **33**, 295401 (2021).
- [72] B. Dóra and C. P. Moca, Quantum Quench in  $\mathcal{PT}$ -Symmetric Luttinger Liquid, *Phys. Rev. Lett.* **124**, 136802 (2020).
- [73] W. Xi, Z.-H. Zhang, Z.-C. Gu, and W.-Q. Chen, Classification of topological phases in one dimensional interacting non-Hermitian systems and emergent unitarity, *Sci. Bull.* **66**, 1731 (2021).
- [74] L. Pan, X. Wang, X. Cui, and S. Chen, Interaction-induced dynamical  $\mathcal{PT}$ -symmetry breaking in dissipative Fermi-Hubbard models, *Phys. Rev. A* **102**, 023306 (2020).
- [75] Z. Xu and S. Chen, Topological Bose-Mott insulators in one-dimensional non-Hermitian superlattices, *Phys. Rev. B* **102**, 035153 (2020).

- [76] T. Hyart and J. L. Lado, Non-Hermitian many-body topological excitations in interacting quantum dots, *Phys. Rev. Research* **4**, L012006 (2022).
- [77] L. Crippa, J. C. Budich, and G. Sangiovanni, Fourth-order exceptional points in correlated quantum many-body systems, *Phys. Rev. B* **104**, L121109 (2021).
- [78] Z. Wang, L.-J. Lang, and L. He, Emergent Mott insulators at noninteger fillings and non-Hermitian conservation laws in an interacting bosonic chain with nonreciprocal hoppings, *Phys. Rev. B* **105**, 054315 (2022).
- [79] A. Banerjee, S.-S. Hegde, A. Agarwala, and A. Narayan, Chiral metals and entrapped insulators in a one-dimensional topological non-Hermitian system, *Phys. Rev. B* **105**, 205403 (2022).
- [80] N. Hatano and D. R. Nelson, Localization Transitions in Non-Hermitian Quantum Mechanics, *Phys. Rev. Lett.* **77**, 570 (1996).
- [81] Here, we are mainly interested in the low- $\text{Re}(E)$  regime of the spectrum. As in Hermitian systems, we refer the ground state to the state with the lowest  $\text{Re}(E)$  and rank the excited states by their  $\text{Re}(E)$  from low to high.
- [82] K. Zhang, Z. Yang, and C. Fang, Universal non-Hermitian skin effect in two and higher dimensions, *Nat. Commun.* **13**, 2496 (2022).
- [83] T. Fukui and N. Kawakami, Breakdown of the Mott insulator: Exact solution of an asymmetric Hubbard model, *Phys. Rev. B* **58**, 16051 (1998).
- [84] See Supplemental Material at <http://link.aps.org/supplemental/10.1103/PhysRevB.106.L121102> for details, which includes Refs. [12,14,15,90,99–101].
- [85] Such a nonreciprocal hopping can be generated in cold-atom systems via synthetic magnetic flux and laser-induced loss; see, e.g., Refs. [48,49].
- [86] We note that, for  $\gamma < 0.03$ , we cannot extrapolate  $U_{\text{TD}}$  accurately with the exact-diagonalization results even up to the largest system size ( $L = 30$ ) that we can achieve in numerics. However, we observe that  $U_{\text{TD}}$  approaches  $2t$  as  $\gamma \rightarrow 0$ .
- [87] I. Affleck and E. H. Lieb, A proof of part of Haldane's conjecture on spin chains, in *Condensed Matter Physics and Exactly Soluble Models* (Springer, New York, 1986), pp. 235–247.
- [88] M. Dalmonte, J. Carrasquilla, L. Taddia, E. Ercolessi, and M. Rigol, Gap scaling at Berezinskii-Kosterlitz-Thouless quantum critical points in one-dimensional Hubbard and Heisenberg models, *Phys. Rev. B* **91**, 165136 (2015).
- [89] In the Hermitian limit, Eq. (1) can be mapped to the XXZ model by Jordan-Wigner transformation.
- [90] N. Byers and C. N. Yang, Theoretical Considerations Concerning Quantized Magnetic Flux in Superconducting Cylinders, *Phys. Rev. Lett.* **7**, 46 (1961).
- [91] We note that a small magnetic flux  $\phi$  will break the  $\mathcal{PT}$  symmetry and generate a small imaginary free energy. Thus the derivative of the free energy with respect to  $\phi$  can be finite, leading to an imaginary persistent current. Imaginary persistent currents in non-Hermitian systems have been reported previously; see, e.g., Refs. [80,96,97]. However, they all focused on single-particle systems without interactions. A persistent current was also obtained within a field theoretical calculation in Ref. [98], which, in contrast to the current obtained in our tight-binding calculation, is real and quantized. Reconciling these results is an interesting question for future work.
- [92] H.-F. Cheung, Y. Gefen, E. K. Riedel, and W.-H. Shih, Persistent currents in small one-dimensional metal rings, *Phys. Rev. B* **37**, 6050 (1988).
- [93] Namely, the number of bonds connecting two simultaneously occupied adjacent sites.
- [94] For small  $U < \Xi_R$ , nontrivial winding numbers and the resulting many-body skin effect can also be found, as we have shown in Fig. S4 in the SM. However, these winding numbers may change as  $U$  changes. The exact relation between these many-body winding numbers and a physical observable remains an open question.
- [95] In many-body fermionic systems, the localization length of eigen wave functions in the presence of open boundaries depends on the particle number  $N$ . When the system is close to half filling and for small  $\gamma$ , the localization length is comparable to  $L$ . In this case, it is hard to observe the localization behavior, as mentioned in Ref. [61]. However, when the localization length is much smaller than  $L$  (i.e., in the case with finite  $N$  and large  $L$  which we are considering), one can observe clearly the localization of all many-body wave functions to an open boundary. This localization behavior becomes constant for increasing  $L$  (but fixed  $N$ ), similar to the non-Hermitian skin effect in single-particle systems.
- [96] N. Hatano and D. R. Nelson, Vortex pinning and non-Hermitian quantum mechanics, *Phys. Rev. B* **56**, 8651 (1997).
- [97] Q. Li, J.-J. Liu, and Y.-T. Zhang, Non-Hermitian Aharonov-Bohm effect in the quantum ring, *Phys. Rev. B* **103**, 035415 (2021).
- [98] K. Kawabata, K. Shiozaki, and S. Ryu, Topological Field Theory of Non-Hermitian Systems, *Phys. Rev. Lett.* **126**, 216405 (2021).
- [99] M. H. Kalthoff, D. M. Kennes, and M. A. Sentef, Floquet-engineered light-cone spreading of correlations in a driven quantum chain, *Phys. Rev. B* **100**, 165125 (2019).
- [100] G. Lindblad, On the generators of quantum dynamical semigroups, *Commun. Math. Phys.* **48**, 119 (1976).
- [101] A. J Daley, Quantum trajectories and open many-body quantum systems, *Adv. Phys.* **63**, 77 (2014).
- [102] D. K. Ferry, R. Akis, A. M. Burke, I. Knezevic, R. Brunner, R. Meisels, F. Kuchar, and J. P. Bird, Open quantum dots: Physics of the non-Hermitian Hamiltonian, *Fortschr. Phys.* **61**, 291 (2013).
- [103] L. L. Zhang, G. H. Zhan, D. Q. Yu, and W. J. Gong, Transport through a non-Hermitian parallel double-quantum-dot structure in the presence of interdot Coulomb interaction, *Fortschr. Phys.* **113**, 558 (2018).
- [104] D. M. Zajac, T. M. Hazard, X. Mi, E. Nielsen, and J. R. Petta, Scalable Gate Architecture for a One-Dimensional Array of Semiconductor Spin Qubits, *Phys. Rev. Applied* **6**, 054013 (2016).
- [105] T. Hensgens, T. Fujita, L. Janssen, X. Li, C. J. Van Diepen, C. Reichl, W. Wegscheider, S. Das Sarma, and J. R Petta, Quantum simulation of a Fermi-Hubbard model using a semiconductor quantum dot array, *Nature (London)* **548**, 70 (2017).

- [106] C. Chin, R. Grimm, P. Julienne, and E. Tiesinga, Feshbach resonances in ultracold gases, *Rev. Mod. Phys.* **82**, 1225 (2010).
- [107] L. Zhou, D. Liu, H. Li, W. Yi, and X. L. Cui, Engineering Non-Hermitian Skin Effect with Band Topology in Ultracold Gases, [arXiv:2111.04196](https://arxiv.org/abs/2111.04196).
- [108] S. Guo, C. Dong, F. Zhang, J. Hu, and Z. Yang, Theoretical Prediction of Non-Hermitian Skin Effect in Ultracold Atom Systems, [arXiv:2111.04220](https://arxiv.org/abs/2111.04220).
- [109] G. Kells, D. Meidan, and A. Romito, Topological transitions with continuously monitored free fermions, [arXiv:2112.09787](https://arxiv.org/abs/2112.09787).
- [110] C. Fleckenstein, A. Zorzato, D. Varjas, E. J. Bergholtz, J. H. Bardarson, and A. Tiwari, Non-Hermitian topology in monitored quantum circuits, *Phys. Rev. Research* **4**, L032026 (2022).
- [111] K. Kawabata, K. Shiozaki, and S. Ryu, Many-body topology of non-Hermitian systems, *Phys. Rev. B* **105**, 165137 (2022).